Materials Advances

ROYAL SOCIETY OF CHEMISTRY

PAPER

View Article Online
View Journal | View Issue

Cite this: *Mater. Adv.*, 2022, 3, 4964

Silver modified copper foam electrodes for enhanced reduction of CO_2 to C_{2+} products†

Chong Wang,[a] Chengdeng Wang,[a] Zhihao Xiong,[a] Jiashuai Wang,[a] Wenyuan Zhang,[a] Haofeng Shi,[a] Donghua Wang,[a] Yousong Gu,[a] Zhiming Bai,*[c] Yan Gao*[b] and Xiaoqin Yan*[a]

Received 18th February 2022,
Accepted 6th May 2022

DOI: 10.1039/d2ma00188h

rsc.li/materials-advances

Electrochemical CO_2 reduction reactions (CO_2RRs) have been recognized as a promising solution to environmental and energy problems due to their ability to convert intermittent renewable electricity into hydrocarbon fuels and value-added chemicals. Copper has a unique ability to electrochemically reduce CO_2 to produce C_{2+} hydrocarbon products compared to other metals. However, it is still suffering from low Faraday efficiency (FE) limitations for specific products. Herein, we have prepared an Ag-modified Cu/CuO–Ag catalyst with a porous structure *via* a galvanic replacement reaction method, which reduced CO_2 to C_{2+} products with the FE of 52.5% at −1.1 V (*vs.* RHE). The experimental results and density functional theory (DFT) calculations show that the addition of Ag in Cu is beneficial to increasing the coverage of *CO on the Cu surface, which can decrease the potential barrier energy of the C–C coupling reaction and favor the generation of C_{2+} products. The results of this study may be helpful to the design of efficient tandem catalysts for electrochemical CO_2 reduction.

Introduction

The rising of CO_2 emissions in the atmosphere due to the combustion of fossil fuels has caused a number of environmental problems, such as the greenhouse effect and sea level rise, which has induced great concern about global climate change.[1,2] Therefore, converting CO_2 into chemicals and fuels not only reduces the carbon dioxide content in the atmosphere but also recovers carbon resources and alleviates the energy crisis.[3–5] Among various CO_2 reduction methods, the electrochemical CO_2 reduction reaction (CO_2RR), especially in aqueous media, is attracting a lot of attention. The electrochemical reduction of CO_2 to small organic molecules with high energy density by using renewable energy has the advantages of high efficiency, controllable selectivity, simple reaction unit and great potential for industrial applications.[6–9]

Nowadays, the common catalysts for the CO_2RR are based on transition metals or their compounds, which have been reported to be used for electrochemical CO_2 reduction to produce different products.[10,11] For example, Au, Ag and Zn are capable of reducing CO_2 to carbon monoxide, while Sn, In and Bi are more inclined to reduce CO_2 to formate.[12–18] Copper has attracted great interest as the only metal material capable of electrochemically converting carbon dioxide to hydrocarbons and alcohols in aqueous solution.[19–21] Unfortunately, Cu-based catalysts still face a series of issues in the reduction of CO_2, such as high overpotential, low current density and low product selectivity.[22] Several strategies have been proposed to improve the properties of Cu-based catalysts, including engineering low-coordinated sites and defects,[23–25] modifying the size and shape of nanostructures,[26,27] and tuning the oxidation state.[22,28,29] For example, it has been reported that a copper catalyst synthesized from the reduction of oxidized Cu showed higher activity and better C_{2+} product selectivity in the electrochemical reduction of carbon dioxide compared with unoxidized copper foil.[30] The results show that the reduced copper oxide electrode can expose more optimized surfaces with edges and steps for the initial activation of carbon dioxide molecules and the dimerization of related intermediates.

Currently, a promising method is to combine copper-based catalysts with second catalysts (such as gold, silver and zinc) to further increase the surface coverage of *CO, which contributes to the formation of C_{2+} products.[31–33] For example, Du *et al.* constructed silver–copper bimetallic catalysts with sharp interfaces *via* sequential precipitation for the efficient production of ethylene. The Faraday efficiency of ethylene production was more than twice that of the pure copper catalyst. DFT

[a] School of Materials Science and Engineering, University of Science and Technology Beijing, Beijing 100083, People's Republic of China. E-mail: xqyan@mater.ustb.edu.cn
[b] Laboratory of Nanomaterials, National Center for Nanoscience and Technology, Beijing, 100190, People's Republic of China. E-mail: gaoyan@nanoctr.cn
[c] School of Civil and Resource Engineering, University of Science and Technology Beijing, Beijing 100083, P. R. China. E-mail: baizhiming2008@126.com

† Electronic supplementary information (ESI) available. See DOI: https://doi.org/10.1039/d2ma00188h

calculation shows that the adsorption energy of CO on Cu is three times that of Ag. The CO molecules are first formed on Ag atoms and then trapped by Cu atoms through the Ag/Cu interface, resulting in a large number of CO molecules aggregated on the Cu side of the Ag/Cu interface. Therefore, the increase of the FE for the C_{2+} products is due to the tandem effect of the silver–copper metal sites near the interface.[34] Although CuAg bimetallic catalysts can improve the C_{2+} product selectivity, the activity is still low and the current density is not sufficient for commercialization.[35] Moreover, the reaction mechanism of converting CO_2 to C_{2+} products over Ag-modified Cu-based catalysts should be further elucidated.

Here, Ag-modified Cu/CuO (Cu/CuO–Ag) catalysts with a porous 3D structure were synthesized by a galvanic replacement reaction (GRR) between Ag^+ and Cu. This special mesoscopic architecture provides the best combination between copper and silver, which dramatically improves the Faraday efficiency and current density of ethylene formation. The electrochemical studies show that Cu/CuO–Ag has good catalytic activity toward the reduction of CO_2, and the FE for C_{2+} reaches 52.5% at −1.1 V (*vs.* RHE), much greater than that of the Cu/CuO catalyst (32.2%). DFT calculation shows that increasing the coverage of *CO on the Cu surface facilitates the C–C dimerization reaction and improves the selectivity of C_{2+} products.

Experimental

Chemicals

All chemicals were used as received unless otherwise stated. Copper foil (Cu, 99.99%, thickness 0.25 mm) and silver nitrate ($AgNO_3$, 99.99%) were purchased from Innochem. Potassium hydrogen carbonate ($KHCO_3$, 99.99%) was purchased from J & K chemical. Sodium chloride (NaCl, 99.9%) was bought from HWRK Chem. Copper(II) sulfate pentahydrate ($CuSO_4 \cdot 5H_2O$) was bought from Aladdin. Nitric acid (HNO_3, 65%), phosphoric acid (H_3PO_4, 85%) and sulfuric acid (H_2SO_4, 98%) were from Sinopharm Chemical Reagent. Nitrogen (N_2, 99.9999%) and carbon dioxide (CO_2, 99.999%) were provided by Beijing Beiwen Gases Company.

Synthesis of electrocatalysts

Preparation of Cu foil electrodes. The copper foil was cut into a size of 1 × 1 cm and cleaned with ethanol, hydrochloric acid and deionized water in 5 min to remove organic matter and the oxidation film on the surface of the copper foil. Then copper foil was used as a working electrode, the platinum mesh was used as the opposite electrode and Ag/AgCl was used as a reference electrode. The polishing was performed in 85% phosphoric acid solution for 30 seconds at a constant voltage of 1.2 V. The copper foil was rinsed three times with deionized water and blown dry with nitrogen.

Preparation of Cu foam electrodes. The preparation of copper foam is according to the previously reported method. A polished Cu foil as the working electrode and a Pt net as the counter electrode were immersed in a solution comprising 1.5 M H_2SO_4, 0.2 M $CuSO_4 \cdot 5H_2O$ and 20 mM NaCl using a DC power supply with a constant current of 2 A cm^{-2} for 15 s. For comparison, Ag foam and Cu–Ag foam were prepared under similar conditions by applying a current of 2 A cm^{-2} for 15 s.

Preparation of Cu/CuO and Cu/CuO–Ag electrodes. The resulting Cu foam has been annealed at 250 °C for 3 h in air in a tube furnace (Lenton) to form Cu/CuO foam. The temperature ramp for heating was 5 °C min^{-1}. $AgNO_3$ and HNO_3 were sequentially dissolved in deionized water to obtain solutions with corresponding concentrations of 25 and 10 mM, respectively. The Cu/CuO foam was soaked into the above solutions for 1, 3 and 5 min to be named Cu/CuO–Ag1, Cu/CuO–Ag, and Cu/CuO–Ag5, respectively.

Characterization of the catalysts

The surface morphology and elemental composition of the catalysts were characterized by scanning electron microscope (Gemini-500) coupled with energy-dispersive X-ray spectroscopy (EDX). The microscopic morphology of the catalysts was further studied by transmission electron microscopy (TEM, FEI TALOS 200X). The crystalline structures and phases were characterized by an X-ray diffractometer (XRD UltimaIV, SmartLab). X-ray photoelectron spectroscopy (XPS, Kratos Axis Ultra spectrometer instrument) was used for analyzing the chemical compositions of the samples. The electrochemically active surface areas (ECSAs) of the Cu foam, Cu/CuO and Cu/CuO–Ag were determined by double layer capacitance measurements. Cyclic voltammetry (CV) measurements were performed from −0.11 V to −0.01 V (*vs.* RHE) at various scan rates in the N_2 saturated state. The non-Faraday current density (Δj) was calculated from the equation $\Delta j = (j_a - j_c)/2$, whereby j_c and j_a are the cathode and anode current densities at −0.06 V *vs.* RHE. Plotting Δj against the scan rate, the slope was determined as the double layer capacitance (C_{DL}) value. The roughness factors were evaluated by the equation $R_F = C_{DL}/C_s$, with C_{DL} of Cu foil as the general C_s.

Electrochemical CO_2 reduction measurements

A CHI660E potentiostat was used for all CO_2 reduction experiments. A specially designed airtight glass electrolytic cell (H-type) was used to conduct the CO_2 electrolysis test. During potentiostatic CO_2 electrolysis, carbon dioxide is continuously injected into the cathode solution at a speed of 30 mL min^{-1} by a Mass Flow Controller (MFC) for gases. Electrodes were pre-reduced for more than 30 min to reduce CuO to Cu at −2.0 V (*vs.* Ag/AgCl). The electrochemical reduction potential of CO_2 was investigated by performing linear sweep voltammetry (LSV) at a scan rate of 50 mV s^{-1} from 0 V to −2.0 V (*vs.* Ag/AgCl). All potentials are reported relative to a reversible hydrogen electrode (RHE) through the below equation:

$$E_{RHE} = E_{(Ag/AgCl)} + 0.205V + 0.059V \times PH_{electrolyte} \quad (1)$$

To evaluate the selectivity of CO_2 reduction, we used online electrochemical gas chromatography (GC, Shimadzu GC-2014c) to detect the gas product during the CO_2RR through the

continuous flow of an electrolytic cell. The GC was calibrated regularly using a standard gas combination under standard circumstances. The faradaic efficiency (FE) data of the gas product was computed from the following equation:

$$\mathrm{FE}\% = (\mathrm{ppm} \times \mathrm{flow\ rate} \times (nFp_0/RT))/j_{\mathrm{Tot}} \times 100\% \quad (2)$$

where ppm is the concentration of the gas phase product measured from GC, flow rate represents the molar flow rate of CO_2 gas measured by a universal flow meter at the outlet of the electrochemical cell, n is the required number of electrons to produce a specific product in the reduction reaction, j_{Tot} is the total current density, p_0 is the ambient pressure, and F is the Faraday constant. Gas composition was analyzed at 15 min intervals during steady-state CO_2 electrolysis according to online measurements.

The electrolytes were collected separately after 1 h of electrolysis at each potential and the liquid products were analyzed quantitatively using the Ascend-400 MHz nuclear magnetic resonance (NMR) spectrometer. After 1 h of electrolysis, 0.5 mL of electrolyte was removed, and 0.1 mL of D_2O and 1.67 ppm of dimethyl sulfoxide (DMSO) were added to it as an internal standard. A pre-saturation technique is used to suppress the water signal. The FE data for liquid products are computed using the following formula:

$$\mathrm{FE}_{\mathrm{liquid}}\% = 1.67nF \times (A/A_0) \times (6/n_{\mathrm{H}}) \times V_{\mathrm{Tot}} \times (Q_{\mathrm{Tot}})^{-1} \times 100\% \quad (3)$$

where the parameters n and F represent the same meaning as the gaseous product in the same way. A_0 represents the peak area of DMSO, A represents the peak area of the liquid product, Q_{Tot} is the amount of total charge transferred during the electrolytic reduction of CO_2, and n_{H} is the proton number relative to the ^{1}H NMR peak of the liquid product.

Density functional theory calculations

All DFT calculations were carried out using the Vienna Ab initio Simulation Package (VASP).[36–38] We used the generalized gradient approximation and the Perdew–Burke–Ernzerhof exchange–correlation functional.[39] The projection enhanced wave (PAW) method was used to deal with the interaction between electrons and ions, and the energy cutoff of the plane wave base was set as 450 eV.[40] A (3 × 3 × 1) Monkhorst–Pack k-point mesh was used to optimize the surface structures. The convergence criteria for residual forces and energies were set to 0.01 eV Å^{-1} and 10^{-4} eV for vacuum spaces greater than 20 Å in the z-direction to avoid interactions between periodic cells during structural relaxation.

We first optimized the crystal structure and found the equilibrium lattice constant to be αCu = 3.631. Then a 4-layer model with a p (3 × 3) Cu(111) supercell was used, with the top two layers relaxed and the bottom two layers fixed. The Nudged Elastic Band (NEB)[41] and Dimer's methods[42] were used to locate the transition state structures, and to further optimize the transition state using a residual force convergence criterion of less than 0.05 eV Å^{-1}.

Results and discussion

The method of preparing Cu/CuO and decorating it with Ag-islands (Cu/CuO–Ag) is shown schematically in Fig. 1. Firstly, the Cu foam was prepared by the hydrogen bubble template method. When high current densities of $j = -2$ A cm^{-2} are applied in the high acid environment (1.5 M H_2SO_4), the hydrogen evolution reaction (HER) is superimposed on the corresponding metal deposition and gas bubbles temporarily appear on the electrode as geometric templates for Cu deposition. The main source of HER in an acidified aqueous solution is proton reduction (eqn (4)) and water splitting (eqn (5)).

$$\mathrm{HER\ (proton\ reduction):}\ 2H^+ + 2e^- \rightarrow H_2 \quad (4)$$

$$\mathrm{HER\ (water\ splitting):}\ 2H_2O + 2e^- \rightarrow H_2 + 2OH^- \quad (5)$$

$$\mathrm{Metal\ deposition:}\ Cu^{2+} + 2e^- \rightarrow Cu_{\mathrm{met}} \quad (6)$$

The morphological characteristics of copper foams after deposition for 20 s are shown in Fig. S1 (ESI†). The original Cu foam shows an obvious pore size gradient along the surface normal. The smallest pore is close to the supporting electrode (copper foil), and the largest pore is located on the outermost surface of the Cu foam. The interconnected pores are visible

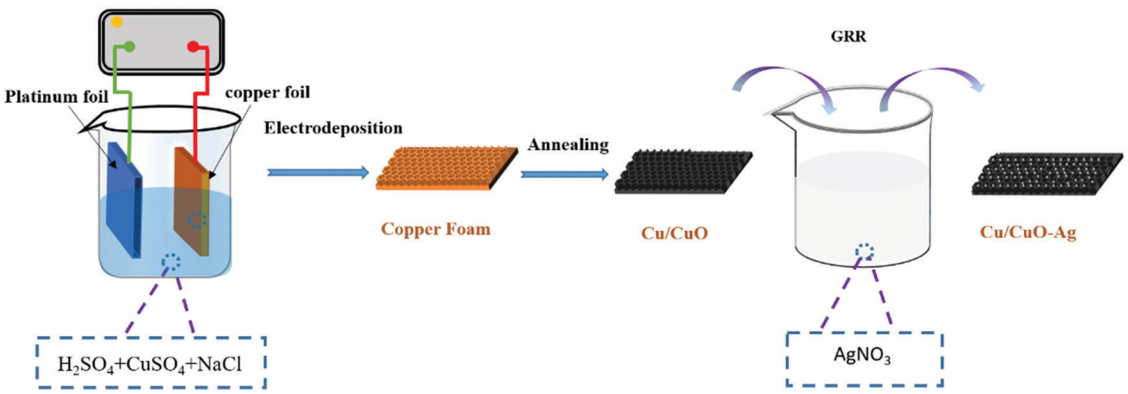

Fig. 1 Schematic route for the preparation of Cu/CuO and Cu/CuO–Ag.

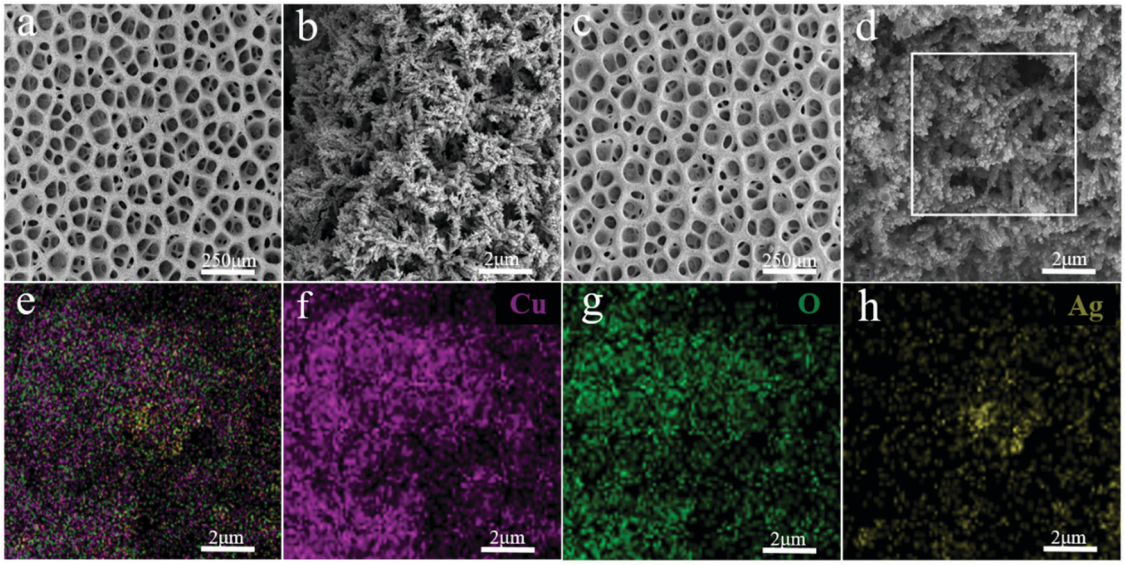

Fig. 2 (a) and (b) SEM images of Cu/CuO. (c) and (d) SEM images of Cu/CuO–Ag. (e–h) EDX images of overlap, Cu, O and Ag of Cu/CuO–Ag.

with surface pore sizes varying from 50 to 80 μm, which provide adequate space for the electrolyte to circulate freely. The sidewalls of the pores are composed of loosely packed copper dendrites, thus forming "secondary" nanopores in the Cu foam. Then, the Cu foam was further thermally annealed in air at 250 °C for 3 h, thereby converting the catalyst materials into Cu/CuO foams. The overall morphology of the copper foam remains essentially unchanged following thermal annealing, which is proved by SEM (Fig. 2a and b). The Cu/Cu_2O–Ag was prepared by immersing Cu/CuO into an aqueous $AgNO_3$ solution for 1–5 min. Since the standard reduction potential of the Cu^{2+}/Cu redox couple (0.34 V *vs.* SHE) is lower than that of Ag^+/Ag (0.80 V *vs.* SHE), the following primary galvanic replacement reaction (GRR) occurs spontaneously:

$$Cu + 2Ag^+ \rightarrow Cu^{2+} + 2Ag \quad (7)$$

After 3 min of GRR in 10 mM $AgNO_3$ solution, silver nanoparticles (NPs) with the size of 50–100 nm were uniformly distributed on the surface of Cu/CuO foams (Fig. 2c and d). The EDX shows that Cu, O and Ag are uniformly distributed in the Cu/CuO–Ag nanocomposites (Fig. 1e–h), which matches well with the results of the above SEM characterizations. The TEM image (Fig. S2, ESI†) shows that silver nanoparticles are attached to copper dendrites. In addition, we also characterized the distribution of Ag nanoparticles in the Cu/CuO–Ag1 and Cu/CuO–Ag5 samples. The images in Fig. S3 (ESI†) show a gradual increase in the average size of the Ag nanoparticles from the Cu/CuO–Ag1 to Cu/CuO–Ag5 samples. The roughness factor of the foam structured catalyst was estimated using the double layer capacitance in the nonfaradaic regions of the CV method. The electrodeposited catalysts have a larger roughness factor than that of the Cu foil catalysts. The roughness of the catalysts follows the order as Cu foam < Cu/CuO–Ag < Cu/CuO (Fig. S4 and Table S1, ESI†).

The XRD of Cu/CuO and Cu/CuO–Ag show peaks that belong to the diffraction of CuO(PDF NO. 45-0793) and Cu(PDF No. 04-0836) (Fig. 3a). The peaks at 38.3°, 44.4°, 64.4° and 77.3° of Cu/CuO–Ag could be ascribed to Ag(111), Ag (200), Ag(220) and Ag(310), respectively. XPS was used to study the chemistry states and surface composition of the Cu/CuO–Ag catalysts. The catalyst exhibits a pair of spin–orbiting double Cu 2p peaks, which may be attributed to Cu $2p_{3/2}$ and Cu $2p_{1/2}$, respectively (Fig. 3b). The fitting peaks at 933.8eV and 953.2 eV are ascribed to the Cu $2p_{3/2}$ and Cu $2p_{1/2}$ peaks of Cu^{2+}, respectively. Furthermore, the presence of CuO is supported by the presence of two discernible shake-up satellite peaks.[43] The fitted peak at 932.1 eV makes it hard to distinguish the Cu^+ and Cu^0 directly by XPS since the difference in binding energy between Cu^+ and Cu^0 is only 0.1 eV.[44] The chemical state of Cu was further verified using Auger electron spectroscopy (Fig. 3c). Cu LMM XAES spectra indicate the presence of two surface Cu species near 914 eV (Cu^+) and 918 eV (Cu^0). The silver $3d_{3/5}$ and $3d_{3/2}$ peaks of the Cu/CuO–Ag are located at 368.6 and 374.6 eV (Fig. 3d), which also confirms the existence of Ag on Cu/CuO–Ag.[45] The Cu/CuO and Cu/CuO–Ag catalysts were also characterized after pre-reduction (Fig. S5, ESI†). It can be confirmed by XRD and XPS that the CuO components have been reduced to Cu in both catalysts.

The selectivity and activity of the CO_2RR were evaluated in a three-electrode H-type cell at a constant external electrode potential (Fig. S6, ESI†). The catalytic activity of the prepared catalysts was first investigated by linear voltammetry. As shown in Fig. 4a, both catalysts exhibit higher current density to reduce CO_2 compared to the copper foil. The total current density of Cu/CuO and Cu/CuO–Ag increases from 1.05 mA cm^{-2} to 18.42 mA cm^{-2} and from 1.45 mA cm^{-2} to 22.76 mA cm^{-2} when the potential decreased from −0.47 V to −1.20 V (*vs.* RHE). Therefore, the total current density of the Cu/CuO and Cu/CuO–Ag

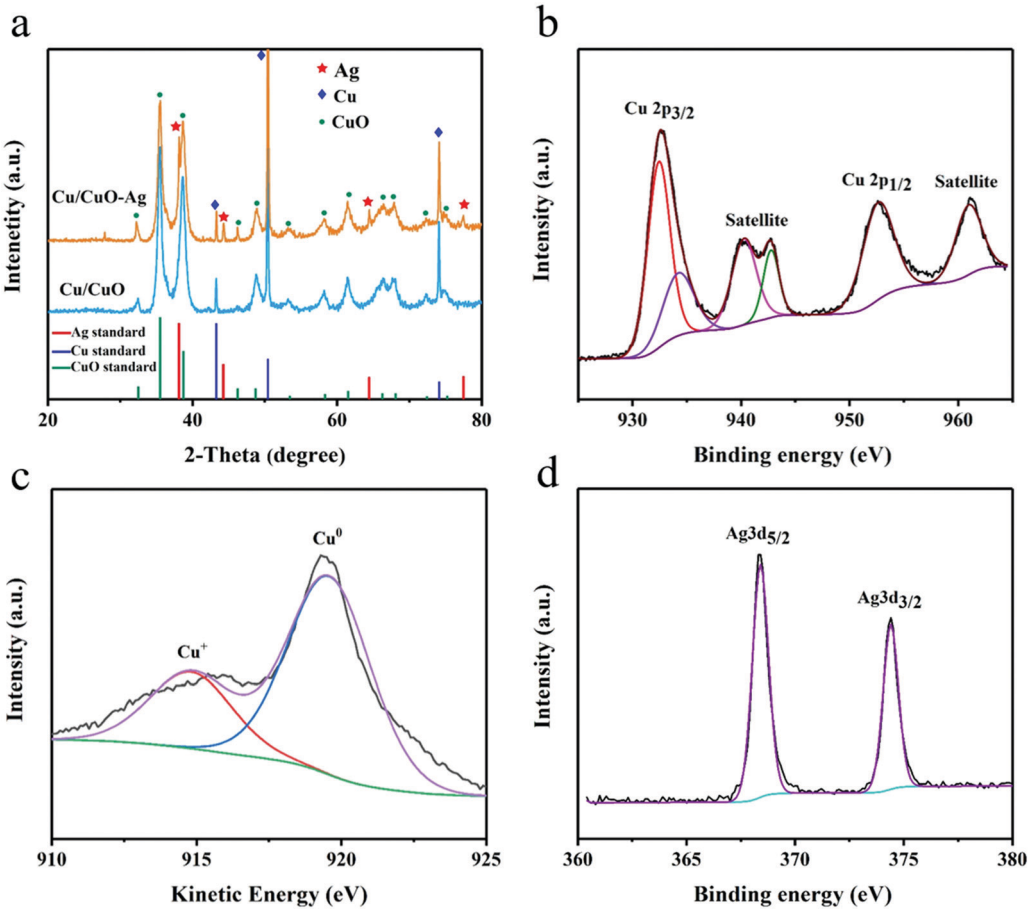

Fig. 3 (a) XRD patterns of Cu/CuO and Cu/CuO–Ag. (b) High-resolution Cu 2p XPS spectra, (c) Auger spectra of Cu LMM, and (d) Ag 3d XPS spectra of Cu/CuO–Ag.

catalysts shows similar trends, but the current density of the Cu/CuO–Ag catalyst is greater than that of the Cu_2O catalyst, which indicates that the introduction of Ag improved the catalytic activity of the catalysts. In addition, the total current density of Cu/CuO is greatly improved compared with the original Cu foam at different potentials (Fig. S8a, ESI†), which may be caused by the significant increase in surface roughness of the Cu foam after annealing reduction (Table S1, ESI†).

The selectivity of the products was obtained by GC and ^{1}H NMR analysis after applying different potentials in a 0.1 M $KHCO_3$ solution with saturated CO_2 and electrolysis at each potential for 1 h. The geometric current density of Cu/CuO–Ag remained stable during 60 min of electrolysis (Fig. S7, ESI†). The FE values of the carbon dioxide reduction products on the Cu/CuO and Cu/CuO–Ag catalysts are shown in Fig. 4b and c. For the Cu/CuO–Ag catalysts, the reduction of CO_2 produced almost no C_{2+} product, and the main product is H_2 with FE of 62.01–56.7% at overpotentials from −0.6 V to −0.7 V (*vs.* RHE). Significantly, the FE of C_2H_4 increases from 13.9% at −0.8 V to 38.7% at −1.1 V (*vs.* RHE). The FE of C_2H_4 for the Cu/CuO–Ag catalyst was 38.7% at −1.2 V (*vs.* RHE), which is greater than the Faraday efficiency of Cu/CuO (22.4%) at the identical potential. By contrast, copper foil and copper foam catalysts produce much fewer C_2H_4 (Fig. S8b, ESI†). The copper foam catalyst generates few hydrocarbons and the major formic acid product exceeds 26% at −1.0 V (*vs.* RHE), which is consistent with the literature.[46] Quite intriguingly, the Faraday efficiency of the formate for the Cu/CuO catalyst has remained at a relatively low level and would not exceed 11% at any electrolytic potential. In contrast, the Faraday efficiencies for ethylene and ethanol products reach 22.4% and 12.8%, respectively.

The key to reducing CO_2 to HCOOH or CO is whether the CO_2 is adsorbed by its oxygen atoms or carbon atoms. There is no breaking of the CO bond during the formation of HCOOH. The CO_2 molecules form $*CO_2^{\bullet-}$ free radical anions on the surface of the catalysts and extract a proton from the adjacent water, which then results in the production of formate.[47] The different distribution of CO_2RR products between Cu foams and Cu/CuO catalysts is mainly due to the weakly coordinated surface sites caused by electrochemical reduction of Cu/CuO foams under CO_2RR conditions, which are particularly active for carbon–carbon coupling reactions.[48]

Fig. 4d summarizes the C_{2+} product FEs for Cu/CuO and Cu/CuO–Ag catalysts. The Ag/Cu catalysts show the highest FEs for the C_{2+} products (52.5% at −1.1 V *vs.* RHE) as compared to Cu/CuO (32.2%), which indicates that the addition of Ag

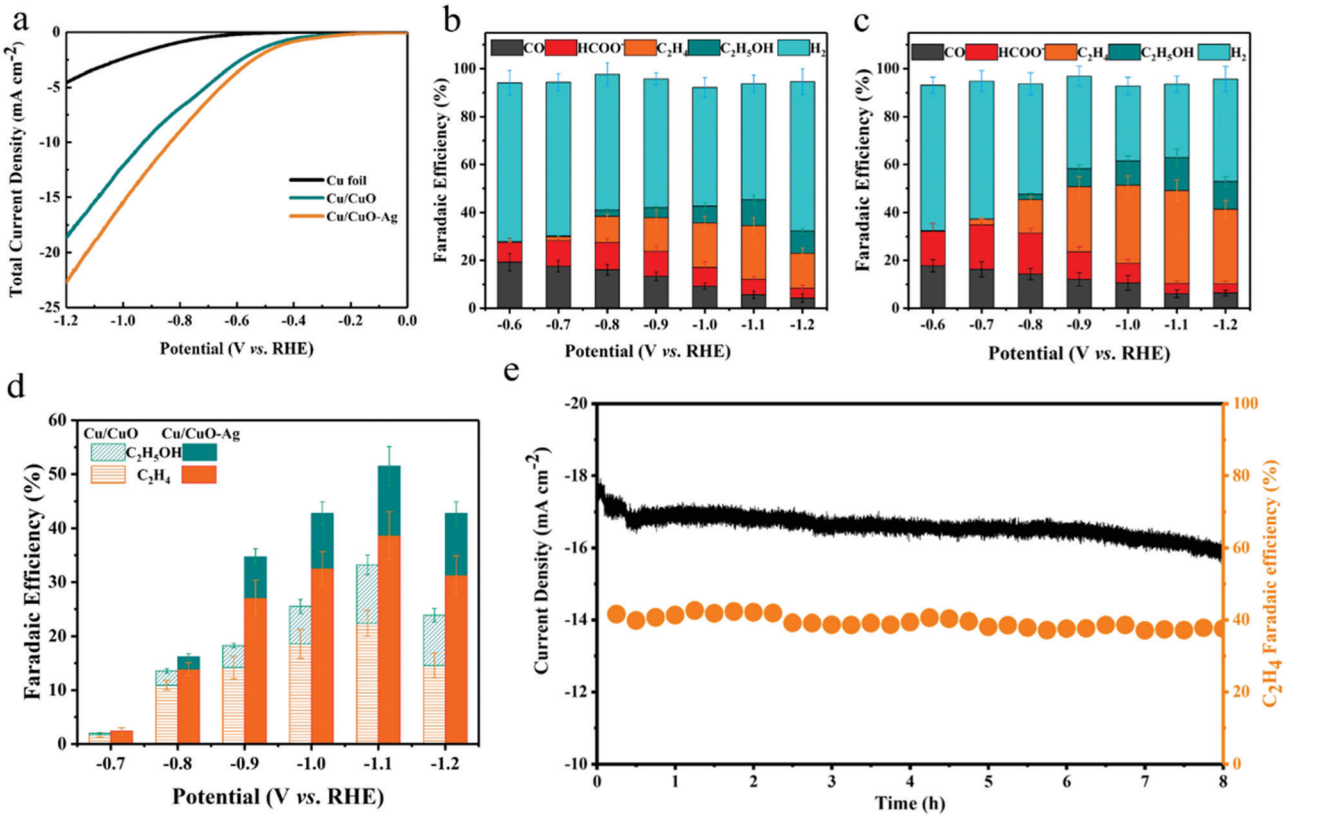

Fig. 4 Electrocatalytic carbon dioxide reduction performance on Cu/CuO, Cu/CuO–Ag and Cu foil catalysts. (a) LSV curves of Cu foil, Cu/CuO and Cu/CuO–Ag. Faraday efficiency for each gaseous product (H_2, CO, C_2H_4) and the main liquid product ($HCOO^-$, C_2H_5OH) over (b) Cu/CuO, and (c) Cu/CuO–Ag in the potential range of −0.8 to −1.2 V (*vs.* RHE). (d) Faraday efficiency for the C_{2+} product of Cu/CuO and Cu/CuO–Ag in the potential range of −0.7 to −1.2 V (*vs.* RHE). (e) The FE of C_2H_4 and total current density of the Cu/CuO–Ag catalyst over 8 hours at −1.1 V (*vs.* RHE).

nanoparticles can efficiently improve the selectivity of the C_{2+} products. We also test the electrochemical reduction characteristics of the Cu/CuO–Ag catalysts by varying the Ag content. FE of the C_{2+} product shows a volcanic variation with increasing Ag loading, which indicates that there is an optimal amount of Ag loading (Fig. S9, ESI†). When the content of Ag is low, it does not provide enough CO intermediates for the copper atoms to promote the C–C coupling reaction. While the higher content of Ag leads to severe aggregation of silver nanoparticles, resulting in elevated FE of CO and lower FE of C_{2+}. Ag foam and Cu–Ag foam were also prepared in a similar way (Fig. S10, ESI†). XRD patterns show that separated pure metal Cu and Ag phases are also formed in the Cu–Ag foam (Fig. S11, ESI†). Their performance for CO_2 reduction was tested under the same conditions (Fig. S12, ESI†), and the CO_2 reduction product on the Ag foam is dominated by CO, yielding a very small amount of C_2H_4 (FE < 3%). In contrast, the selectivity of the Cu–Ag foam for the C_{2+} product is significantly improved, reaching a Faraday efficiency of 27.5% for the C_{2+} product at −1.1 V (*vs.* RHE). However, it is lower than that of Cu/CuO–Ag (52.5%), indicating that the synergistic effect between the oxidation-derived Cu and Ag modifications leads to the high selectivity of the Cu/CuO–Ag catalyst for the C_{2+} product.

Cu/CuO–Ag shows good stability with continuous reduction of CO_2 to C_2H_4 at −1.1 V (*vs.* RHE) for 8 h (Fig. 4e). The FE 39% of the C_2H_4 products remains almost unchanged. A longer test was conducted for 20 h, and the catalytic activity of Cu/CuO–Ag and the faradaic efficiency for ethylene hardly changes (Fig. S13, ESI†). In addition, the Cu/CuO–Ag catalyst remains in its original porous morphology (Fig. S14, ESI†), which indicates that the Cu/CuO–Ag catalyst has excellent stability.

The FE of C_2H_4 for the Cu/CuO–Ag catalyst is obviously higher than that of the Cu/CuO catalyst, which indicates that the introduction of Ag contributes to the production of C_{2+} products. Furthermore, we discuss the possible catalytic mechanism of reducing CO_2 to C_2H_4 in this catalyst (Fig. 5a). At present, *CO is recognized as a critical intermediary in the electrochemical reduction of carbon dioxide to hydrocarbons.[49] The formation of *CO intermediates from CO_2 molecules usually undergoes two processes. First, the CO_2 molecule is caught by Cu and Ag atoms, and both a proton and an electron are transferred.[50]

$$CO_2 + * + (H^+ + e^-) \rightarrow *COOH \quad (11)$$

Next, the *COOH intermediate is further reduced to *CO.

$$*COOH + (H^+ + e^-) \rightarrow *CO + H_2O \quad (12)$$

Ag atoms are more active than Cu atoms in the production of carbon monoxide molecules.[51] The *CO generated on Ag is

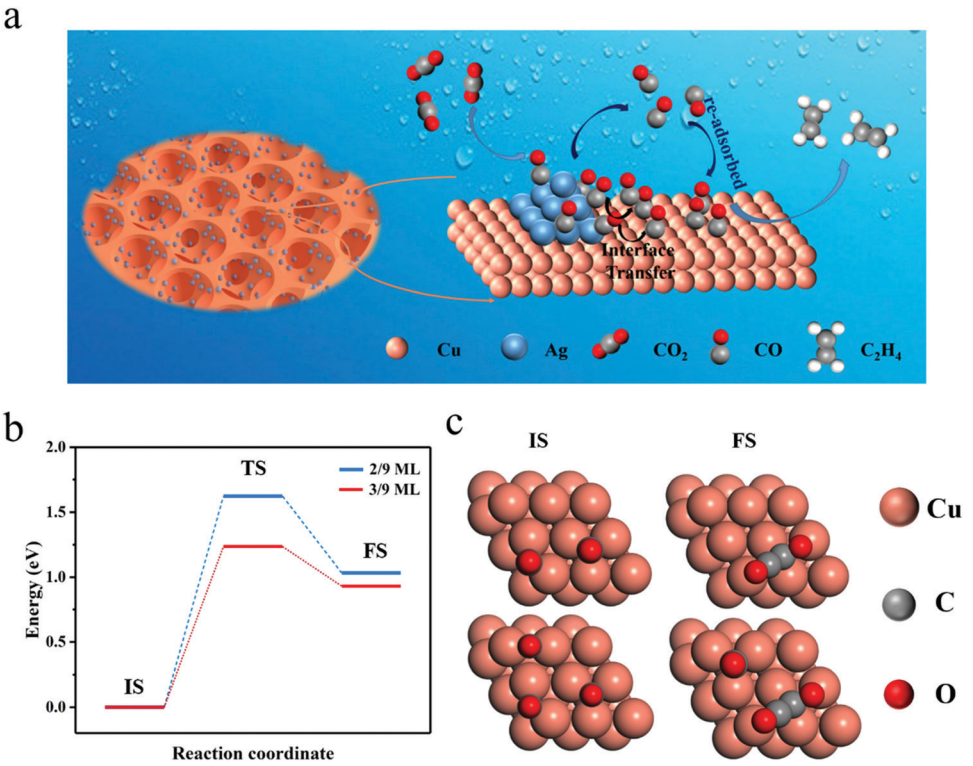

Fig. 5 (a) Mechanism for the electrochemical reduction of CO_2 to ethylene on the Cu/CuO–Ag catalyst. (b) The activation energy barrier of carbon CO at different *CO coverages. (c) The corresponding configurations of the initial state and final state on the CO coverage of 2/9 ML and 3/9 ML. IS, initial state; TS, transition state; FS, final state.

more easily desorbed as *CO is weakly bound to Ag, increasing the local CO concentration around the electrode surface. The CO will be temporarily trapped in the pores of the foam catalyst and re-adsorbed by the Cu sites. Additionally, the *CO intermediate produced on the Ag atoms can be captured by the Cu atoms through the Cu–Ag interface, leading to a high surface coverage of *CO. In the step of further reduction of the CO intermediate to ethylene on the Cu surface, the rate-determining step (RDS) is the dimerization of CO leading to the formation of a C–C bond.[52] We consider that the coverage of CO intermediates on the catalyst surface has an important effect on the CO dimerization reaction and high surface coverage of *CO may facilitate the synthesis of the C_{2+} product, which is further proved by DFT calculation below.

Computationally, a $(3 \times 3 \times 4)$ Cu(111) supercell was built to simulate the catalyst. With DFT, we calculated the C–C coupling barrier energy for *CO coverage of 2/9 ML and 3/9 ML to simulate the effect of high and low* CO coverage on the Cu surface for the synthesis of C_{2+} products (Fig. S15, ESI†), respectively. Although solvent molecules have a certain effect on the CO_2RR,[53] in order to simplify the model, we ignore the role of solvent molecules, and here the geometry of *OCCO is stable, the same as that under no charged water layer.[52] As shown in Fig. 5b and c, increasing the CO coverage from 2/9 ML to 3/9 ML decreases the barrier from 1.62 eV to 1.13 eV, a reduction of 0.49 eV. The lowering of the barrier energy of the C–C coupling reaction is due to the interaction between the adsorbates (CO), which weakens the carbon bonds on the surface and makes the carbon–carbon bonds more easily formed (Table S2, ESI†).

Conclusion

In summary, we have successfully prepared Cu/CuO–Ag catalysts with porous structures using a galvanic replacement method and investigated their catalytic activity for the electrochemical reduction of CO_2. The selectivity of CO_2 reduction to ethylene was significantly improved by the synergistic effect of oxide-derived copper and Ag metals modified on the copper surface. The Faraday efficiency of ethylene reaches 38.6% at −1.1 V (*vs.* RHE) and remains stable over 8 h. Compared to Cu/CuO catalysts, the Cu/CuO-Ag displays better electrochemical performance for the reduction of CO_2 to ethylene, which is due to the efficient spillover of CO from Ag to the Cu surface. DFT calculations indicate that the high CO coverage on the Cu surface decreases the C–C coupling barrier energy and facilitates the formation of C_{2+} products. In addition, the porous structure of the Cu/CuO–Ag catalyst facilitates readsorption of the intermediate CO by the Cu surface for further reduction to C_{2+} products. This work shows strategies for developing efficient Cu-based bimetallic catalysts for the selective formation of C_{2+} products in CO_2RR processes and provides greater insight into the catalyst design for the electrochemical reduction of CO_2.

Author contributions

The manuscript was written through contributions of all authors. All authors have given approval to the final version of the manuscript.

Conflicts of interest

There are no conflicts to declare.

Acknowledgements

This work was supported by the Natural Science Foundation of China (NSFC) (No. 51772024, X. Q. Y.; 51772057, Y. G.).

References

1 Y. Wang, J. Liu, Y. Wang, A. M. Al-Enizi and G. Zheng, Tuning of CO_2 Reduction Selectivity on Metal Electrocatalysts, *Small*, 2017, **13**, 1701809.
2 O. S. Bushuyev, P. De Luna, C. T. Dinh, L. Tao, G. Saur, J. van de Lagemaat, S. O. Kelley and E. H. Sargent, What Should We Make with CO_2 and How Can We Make It?, *Joule*, 2018, **2**, 825–832.
3 D. T. Whipple and P. J.-A. Kenis, Prospects of CO_2 Utilization *via* Direct Heterogeneous Electrochemical Reduction, *J. Phys. Chem. Lett.*, 2010, **1**, 3451–3458.
4 Y. Y. Birdja, E. Pérez-Gallent, M. C. Figueiredo, A. J. Göttle, F. Calle-Vallejo and M. T.-M. Koper, Advances and challenges in understanding the electrocatalytic conversion of carbon dioxide to fuels, *Nat. Energy*, 2019, **4**, 732–745.
5 J. Shi, Y. Jiang, Z. Jiang, X. Wang, X. Wang, S. Zhang, P. Han and C. Yang, Enzymatic conversion of carbon dioxide, *Chem. Soc. Rev.*, 2015, **44**, 5981–6000.
6 J. Qiao, Y. Liu, F. Hong and J. Zhang, A review of catalysts for the electroreduction of carbon dioxide to produce low-carbon fuels, *Chem. Soc. Rev.*, 2014, **43**, 631–675.
7 S. Chu, Y. Cui and N. Liu, The path towards sustainable energy, *Nat. Mater.*, 2016, **16**, 16–22.
8 L. Zhang, Z. J. Zhao and J. Gong, Nanostructured Materials for Heterogeneous Electrocatalytic CO_2 Reduction and their Related Reaction Mechanisms, *Angew. Chem., Int. Ed.*, 2017, **56**, 11326–11353.
9 B. Kumar, J. P. Brian, V. Atla, S. Kumari, K. A. Bertram, R. T. White and J. M. Spurgeon, New trends in the development of heterogeneous catalysts for electrochemical CO_2 reduction, *Catal. Today*, 2016, **270**, 19–30.
10 A. Bagger, W. Ju, A. S. Varela, P. Strasser and J. Rossmeisl, Electrochemical CO_2 Reduction: A Classification Problem, *ChemPhysChem*, 2017, **18**, 3266–3273.
11 L. Hou, J. Yan, L. Takele, Y. Wang, X. Yan and Y. Gao, Current progress of metallic and carbon-based nanostructure catalysts towards the electrochemical reduction of CO_2, *Inorg. Chem. Front.*, 2019, **6**, 3363–3380.
12 A. J. Welch, J. S. DuChene, G. Tagliabue, A. Davoyan, W.-H. Cheng and H. A. Atwater, Nanoporous Gold as a Highly Selective and Active Carbon Dioxide Reduction Catalyst, *ACS Appl. Energy Mater.*, 2018, **2**, 164–170.
13 S.-Q. Liu, S.-W. Wu, M.-R. Gao, M.-S. Li, X.-Z. Fu and J.-L. Luo, Hollow Porous Ag Spherical Catalysts for Highly Efficient and Selective Electrocatalytic Reduction of CO_2 to CO, *ACS Sustainable Chem. Eng.*, 2019, **7**, 14443–14450.
14 J. Rosen, G. S. Hutchings, Q. Lu, R. V. Forest, A. Moore and F. Jiao, Electrodeposited Zn Dendrites with Enhanced CO Selectivity for Electrocatalytic CO_2 Reduction, *ACS Catal.*, 2015, **5**, 4586–4591.
15 N. Han, P. Ding, L. He, Y. Li and Y. Li, Promises of Main Group Metal–Based Nanostructured Materials for Electrochemical CO_2 Reduction to Formate, *Adv. Energy Mater.*, 2019, **10**, 1902338.
16 N. Han, Y. Wang, H. Yang, J. Deng, J. Wu, Y. Li and Y. Li, Ultrathin bismuth nanosheets from in situ topotactic transformation for selective electrocatalytic CO_2 reduction to formate, *Nat. Commun.*, 2018, **9**, 1320.
17 Z. B. Hoffman, T. S. Gray, K. B. Moraveck, T. B. Gunnoe and G. Zangari, Electrochemical Reduction of Carbon Dioxide to Syngas and Formate at Dendritic Copper–Indium Electrocatalysts, *ACS Catal.*, 2017, **7**, 5381–5390.
18 W. Ma, S. Xie, X. G. Zhang, F. Sun, J. Kang, Z. Jiang, Q. Zhang, D. Y. Wu and Y. Wang, Promoting electrocatalytic CO_2 reduction to formate via sulfur-boosting water activation on indium surfaces, *Nat. Commun.*, 2019, **10**, 892.
19 S. Nitopi, E. Bertheussen, S. B. Scott, X. Liu, A. K. Engstfeld, S. Horch, B. Seger, I. E.-L. Stephens, K. Chan, C. Hahn, J. K. Norskov, T. F. Jaramillo and I. Chorkendorff, Progress and Perspectives of Electrochemical CO_2 Reduction on Copper in Aqueous Electrolyte, *Chem. Rev.*, 2019, **119**, 7610–7672.
20 K. P. Kuhl, E. R. Cave, D. N. Abram and T. F. Jaramillo, New insights into the electrochemical reduction of carbon dioxide on metallic copper surfaces, *Energy Environ. Sci.*, 2012, **5**, 7050–7059.
21 Z. Ni, H. Liang, Z. Yi, R. Guo, C. Liu, Y. Liu, H. Sun and X. Liu, Research progress of electrochemical CO_2 reduction for copper-based catalysts to multicarbon products, *Coord. Chem. Rev.*, 2021, **441**, 213983.
22 A. H. Shah, Y. Wang, S. Hussain, M. B. Akbar, A. R. Woldu, X. Zhang and T. He, New aspects of C2 selectivity in electrochemical CO2 reduction over oxide-derived copper, *Phys. Chem. Chem. Phys.*, 2020, **22**, 2046–2053.
23 Z. Wang, G. Yang, Z. Zhang, M. Jin and Y. Yin, Selectivity on Etching: Creation of High-Energy Facets on Copper Nanocrystals for CO_2 Electrochemical Reduction, *ACS Nano*, 2016, **10**, 4559–4564.
24 B. Zhang, J. Zhang, M. Hua, Q. Wan, Z. Su, X. Tan, L. Liu, F. Zhang, G. Chen, D. Tan, X. Cheng, B. Han, L. Zheng and G. Mo, Highly Electrocatalytic Ethylene Production from CO_2 on Nanodefective Cu Nanosheets, *J. Am. Chem. Soc.*, 2020, **142**, 13606–13613.
25 F. Pan and Y. Yang, Designing CO_2 reduction electrode materials by morphology and interface engineering, *Energy Environ. Sci.*, 2020, **13**, 2275–2309.

26 R. Reske, H. Mistry, F. Behafarid, B. Roldan Cuenya and P. Strasser, Particle size effects in the catalytic electroreduction of CO_2 on Cu nanoparticles, *J. Am. Chem. Soc.*, 2014, **136**, 6978–6986.

27 J. J. Lv, M. Jouny, W. Luc, W. Zhu, J. J. Zhu and F. Jiao, A Highly Porous Copper Electrocatalyst for Carbon Dioxide Reduction, *Adv. Mater.*, 2018, **30**, 1803111.

28 M. Favaro, H. Xiao, T. Cheng, W. A. Goddard, 3rd, J. Yano and E. J. Crumlin, Subsurface oxide plays a critical role in CO2 activation by Cu(111) surfaces to form chemisorbed CO_2, the first step in reduction of CO_2, *Proc. Natl. Acad. Sci. U. S. A.*, 2017, **114**, 6706–6711.

29 S. Wang, T. Kou, S. E. Baker, E. B. Duoss and Y. Li, Recent progress in electrochemical reduction of CO_2 by oxide-derived copper catalysts, *Mater. Today Nano*, 2020, **12**, 100096.

30 D. Ren, Y. Deng, A. D. Handoko, C. S. Chen, S. Malkhandi and B. S. Yeo, Selective Electrochemical Reduction of Carbon Dioxide to Ethylene and Ethanol on Copper(I) Oxide Catalysts, *ACS Catal.*, 2015, **5**, 2814–2821.

31 J. Huang, M. Mensi, E. Oveisi, V. Mantella and R. Buonsanti, Structural Sensitivities in Bimetallic Catalysts for Electrochemical CO_2 Reduction Revealed by Ag–Cu Nanodimers, *J. Am. Chem. Soc.*, 2019, **141**, 2490–2499.

32 Y. Zhu, X. Cui, H. Liu, Z. Guo, Y. Dang, Z. Fan, Z. Zhang and W. Hu, Tandem catalysis in electrochemical CO_2 reduction reaction, *Nano Res.*, 2021, **14**, 4471–4486.

33 L. Hou, J. Han, C. Wang, Y. Zhang, Y. Wang, Z. Bai, Y. Gu, Y. Gao and X. Yan, Ag nanoparticle embedded Cu nanoporous hybrid arrays for the selective electrocatalytic reduction of CO_2 towards ethylene, *Inorg. Chem. Front.*, 2020, **7**, 2097–2106.

34 J. Wang, Z. Li, C. Dong, Y. Feng, J. Yang, H. Liu and X. Du, Silver/Copper Interface for Relay Electroreduction of Carbon Dioxide to Ethylene, *ACS Appl. Mater. Interfaces*, 2019, **11**, 2763–2767.

35 M. Jouny, W. Luc and F. Jiao, General Techno-Economic Analysis of CO_2 Electrolysis Systems, *Ind. Eng. Chem. Res.*, 2018, **57**, 2165–2177.

36 G. Kresse and J. Hafner, Ab initio molecular-dynamics simulation of the liquid-metal-amorphous-semiconductor transition in germanium, *Phys. Rev. B: Condens. Matter Mater. Phys.*, 1994, **49**, 14251–14269.

37 G. Kresse and J. Hafner, Ab initio molecular dynamics for liquid metals, *Phys. Rev. B: Condens. Matter Mater. Phys.*, 1993, **47**, 558–561.

38 G. G. Kresse and J. J. Furthmüller, Efficient Iterative Schemes for Ab Initio Total-Energy Calculations Using a Plane-Wave Basis Set, *Phys. Rev. B: Condens. Matter Mater. Phys.*, 1996, **54**, 11169.

39 J. Perdew, K. Burke and M. Ernzerhof, Generalized gradient approximation made simple, *Phys. Rev.*, 1996, **77**, 3856, 1997.

40 P. E. Blochl, Projector augmented-wave method, *Phys. Rev. B: Condens. Matter Mater. Phys.*, 1994, **50**, 17953–17979.

41 S. A. Trygubenko and D. J. Wales, A doubly nudged elastic band method for finding transition states, *J. Chem. Phys.*, 2004, **120**, 2082–2094.

42 D. Sheppard, R. Terrell and G. Henkelman, A dimer method for finding saddle points on high dimensional potential surfaces using only first derivatives, *J. Chem. Phys.*, 2008, **111**, 7010.

43 F. Du, Q.-Y. Chen and Y.-H. Wang, Effect of annealing process on the heterostructure CuO/Cu_2O as a highly efficient photocathode for photoelectrochemical water reduction, *J. Phys. Chem. Solids*, 2017, **104**, 139–144.

44 T. Ghodselahi, M. A. Vesaghi, A. Shafiekhani, A. Baghizadeh and M. Lameii, XPS study of the Cu@Cu_2O core-shell nanoparticles, *Appl. Surf. Sci.*, 2008, **255**, 2730–2734.

45 Y. Mou, H. Wang, Y. Peng, J. Liu, H. Cheng, Q. Sun and M. Chen, Low temperature enhanced flexible conductive film by Ag flake/ion composite ink, *Mater. Des.*, 2020, **186**, 108339.

46 S. Sen, D. Liu and G. T.-R. Palmore, Electrochemical Reduction of CO_2 at Copper Nanofoams, *ACS Catal.*, 2014, **4**, 3091–3095.

47 Y. Zhong, S. Wang, M. Li, J. Ma, S. Song, A. Kumar, H. Duan, Y. Kuang and X. Sun, Rational design of copper-based electrocatalysts and electrochemical systems for CO_2 reduction: From active sites engineering to mass transfer dynamics, *Mater. Today Phys.*, 2021, **18**, 100354.

48 A. Dutta, M. Rahaman, N. C. Luedi and P. Broekmann, Morphology Matters: Tuning the Product Distribution of CO_2 Electroreduction on Oxide-Derived Cu Foam Catalysts, *ACS Catal.*, 2016, **6**, 3804–3814.

49 C. Zhan, F. Dattila, C. Rettenmaier, A. Bergmann, S. Kuhl, R. Garcia-Muelas, N. Lopez and B. R. Cuenya, Revealing the CO Coverage-Driven C–C Coupling Mechanism for Electrochemical CO_2 Reduction on Cu_2O Nanocubes via Operando Raman Spectroscopy, *ACS Catal.*, 2021, **11**, 7694–7701.

50 A. A. Peterson, F. Abild-Pedersen, F. Studt, J. Rossmeisl and J. K. Norskov, How copper catalyzes the electroreduction of carbon dioxide into hydrocarbon fuels, *Energy Environ. Sci.*, 2010, **3**, 1311–1315.

51 J. T. Feaster, C. Shi, E. R. Cave, T. Hatsukade, D. N. Abram, K. P. Kuhl, C. Hahn, J. K. Nørskov and T. F. Jaramillo, Understanding Selectivity for the Electrochemical Reduction of Carbon Dioxide to Formic Acid and Carbon Monoxide on Metal Electrodes, *ACS Catal.*, 2017, **7**, 4822–4827.

52 F. Calle-Vallejo and M. T. Koper, Theoretical considerations on the electroreduction of CO to C2 species on Cu(100) electrodes, *Angew. Chem., Int. Ed.*, 2013, **52**, 7282–7285.

53 X. Hu, S. Yao, L. Chen, X. Zhang, M. Jiao, Z. Lu and Z. Zhou, Understanding the role of axial O in CO_2 electroreduction on NiN_4 single-atom catalysts via simulations in realistic electrochemical environment, *J. Mater. Chem. A*, 2021, **9**, 23515–23521.